

Article

Low Profile Sinuous Slot Antenna for UWB Sensor Networks

Ján Gamec ¹, Miroslav Repko ¹ , Mária Gamcová ¹ , Iveta Gladišová ¹ , Pavol Kurdel ², Alexey Nekrasov ^{3,4,5,*}  and Colin Fidge ⁵

¹ Faculty of Electrical Engineering and Informatics, Technical University of Košice, Letná 9, Košice 042 00, Slovakia; jan.gamec@tuke.sk (J.G.); miroslav.repko@tuke.sk (M.R.); maria.gamcova@tuke.sk (M.G.); iveta.gladisova@tuke.sk (I.G.)

² Faculty of Aeronautics, Technical University of Košice, Rampová 7, Košice 041 21, Slovakia; pavol.kurdel@tuke.sk

³ Institute for Computer Technologies and Information Security, Southern Federal University, Chekhova 2, Taganrog 347922, Russia

⁴ Department of Radio Engineering Systems, Saint Petersburg Electrotechnical University, Professora Popova 5, Saint Petersburg 197376, Russia

⁵ Science and Engineering Faculty, Queensland University of Technology, Gardens Point Campus, Brisbane QLD 4001, Australia; c.fidge@qut.edu.au

* Correspondence: alexei-nekrassov@mail.ru; Tel.: +7-8634-360-484

Received: 24 December 2018; Accepted: 21 January 2019; Published: 25 January 2019



Abstract: This article describes the design and implementation of a low-profile sinuous slot antenna, intended for ultra-wideband (UWB) sensor networks, which can be produced on one conductive layer. The article explains the design and optimization of the sinuous slot antenna and its modifications, including its sinusoidal curve shape. Other modifications were aimed at optimizing the antenna feeding. Desirable properties of the designed and implemented antenna modifications were verified both by simulation and empirically. Experimental measurements of the antenna's properties were carried out using a vector network analyzer in an anechoic chamber and also by a pulsed UWB radar in the frequency range from 0.1 to 6 GHz. The low-profile antennas were implemented on a Rogers RO3206 substrate.

Keywords: sinuous antenna; slot antenna; low-profile antenna; UWB antenna

1. Introduction

At present, ultra-wideband (UWB) radar systems appear to be an appropriate tool in many applications [1,2]. They are capable of non-invasive motion detection, while their broadband properties provide them with sufficient precision for their application as contactless heart sensing or breathing sensors [3]. UWB radars can also be used for many other applications, such as medicine, civil engineering, impedance spectroscopy [4], ground penetrating radar (GPR) applications [5], through-wall security applications [6], and many others [7]. Additionally, UWB technology is currently widely used in sensor networks, providing high robustness to interference as well as a low complexity of transmitters and receivers while decreasing the energy consumption. The IEEE 802.15.4a standard defines UWB-based sensor networks as having a high degree of flexibility, including their modulation, coding, and multiple access schemes. Antennas and their properties are the key elements in the field of sensors [8]. In some applications, in addition to their large bandwidth and electrical characteristics, their dimensions are also critical. Examples of such applications are wearable devices [9] or energy harvesting [10,11].

This article presents the design of a UWB antenna for through-wall measurements in security applications. The requirements for such an antenna include minimum ringing and a bandwidth greater than 500 MHz, or 0.2 times the central frequency in a relative form [12]. Other requirements include linear polarization, the width of the main lobes being more than 90°, a low-profile structure, easy implementation combined with low production costs, and minimum dimensions for the use of frequencies lower than 0.8 GHz.

The shape of the proposed antenna is based on sinuous curves drawn in the polar coordinate system. The curve of this antenna was originally designed in the 1980s by R. H. Duhamel [13]. Its main advantage is that it is an analytical curve and it allows the creation of logarithmically periodic structures and shapes. Just the log-periodic structure of the antenna allows it to achieve a large frequency bandwidth in a compact and planar shape.

A number of recent publications describe similar UWB antennas [14–19], but these solutions do not work at such low frequencies and do not achieve such a large relative bandwidth and compact dimensions as our solution presented below.

This form of antenna has been known for several decades, but in a non-planar form [20,21]. The main purpose of the new design was to modify the UWB sinuous antenna for radar systems with linear polarization. A large relative width of the frequency band and frequencies below 0.8 GHz allow its electromagnetic waves better penetration and transmission through walls. The production of the antenna itself and its excitation in planar form at a low production cost, using inexpensive technological processes and dielectric materials, favor this antenna in the construction of light and portable systems.

The antenna was implemented in a slotted form. This means that the antenna is etched or milled into the conductive layer of a printed circuit board (PCB) substrate. In the same layer in which the antenna is produced, the excitation of the antenna is included as a coplanar waveguide (CPW). It should be noted that the resulting slot antennas have a polarization vector oriented perpendicular to the axis of the main arms of the slot.

2. Design of the Antenna Geometry

2.1. Basic Shape

The sinuous shape introduced by Duhamel [13] provides a logarithmically periodic structure of an antenna pattern that is theoretically frequency-independent. Thanks to this feature, the sinuous form (analytical curve) is suitable for tuning and producing an antenna suitable for UWB radar systems.

In general, the antenna consists of N arms consisting of P incrementally growing cells. The size of the p -th cell grows (scaling) from the first cell (inner cell—the smallest and closest to the center) to the last cell (outer cell—the largest and closest to the outer edge). The symbols r_p and r_{p+1} denote the inner and outer radii of the p -th cell. The sinusoidal curve (in the polar coordinate system) that is the basis for the shape of the antenna can be described by the following equation [13,19]:

$$\Phi_p(r) = (-1)^{p-1} \alpha_p \sin \left(\pi \frac{\ln \left(\frac{r}{r_p} \right)}{\ln(\tau_p)} \right), r_p \leq r \leq r_{p+1} \quad (1)$$

where α_p and τ_p are the key design parameters. Parameter α_p is a positive number that defines the maximum value of Φ in a cell via the index p , in which half of the sinusoidal wave curve in the polar system is present. Parameter τ_p defines the so-called cell growth. Such a sinusoidal curve fulfills the logarithmic periodicity condition, thereby achieving the theoretical frequency independence of the antenna's bandwidth. Parameter τ_p is defined as the ratio of the outer and inner radii [13]:

$$\tau_p = r_{p+1}/r_p \quad (2)$$

Parameters α_p and τ_p are usually unchanged for the entire antenna.

The slot contour curve of one antenna arm is then formed from two sinuous curves by rotating them with a defined angle ($\pm\delta$). In Figure 1, it is possible to see a basic curve with one cell highlighted (bold curve).

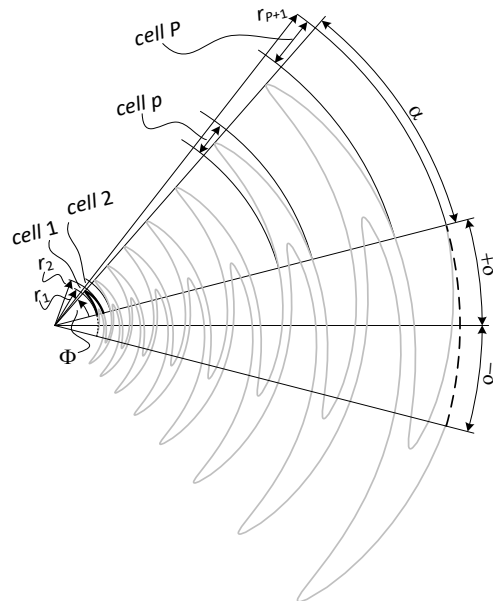


Figure 1. An arm of the antenna and its geometry.

The total sinusoidal curve is created by joining individual cells (gray curve in Figure 1). By adding additional curves and by their mutual rotation by the angles of $+\delta$ and $-\delta$, an arm of the antenna is created. It is terminated at both ends by the arc (dashed curves). The radius of the inner circle is r_1 and the length of the arc is 2δ . The radius of the outer circle is $r_1\tau^P$ and the angular length of the arc is 2δ as well. The second arm of the antenna arises by simply rotating the first arm by an angle of π rad.

For localizing moving objects behind a barrier, an electromagnetic field with linear polarization is often used [6,12,22–24]. For this reason, the resulting antenna consists of only two arms ($N = 2$), as shown in Figure 2. When N is greater than 2, the sinuous antenna is able to provide two patterns with orthogonal linear polarizations [13,19,25,26].

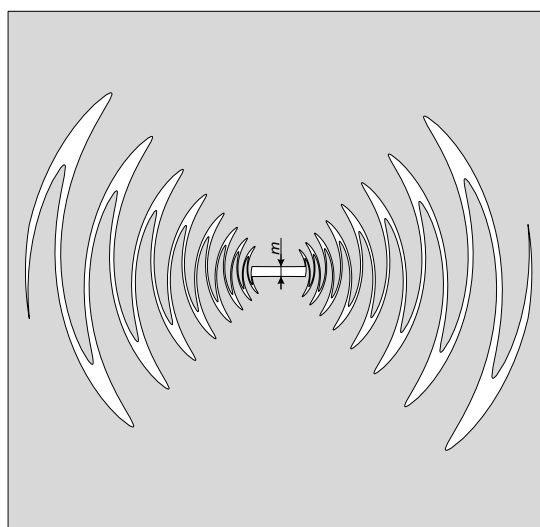


Figure 2. The two arms of the sinuous slot antenna.

The analytical equation of the curve, Equation (1) above, was transformed from a polar to a Cartesian form to support its use in the CST MicroWave Studio (CST MWS) simulation environment. The resulting curve equation can thus be written as:

$$X_p(t) = t \cos(\Phi_p(t)), \tag{3}$$

$$Y_p(t) = t \sin(\Phi_p(t)) \tag{4}$$

where t is in the range $\langle r_1 \tau^{p-1}, r_1 \tau^p \rangle$ in each cell, with an index of p , α is the cell's angular width, r_1 is the smallest antenna radius, and τ is the cell growth index.

2.2. Antenna Ripple

The main idea of modifying the antenna by forming ripples on its cells is to increase the antenna's bandwidth towards lower frequencies while maintaining the same outer dimensions [26]. The antenna cells' ripples cause extensions of surface current pathways. Figure 3 compares the contour curves of an antenna cell with and without a ripple.

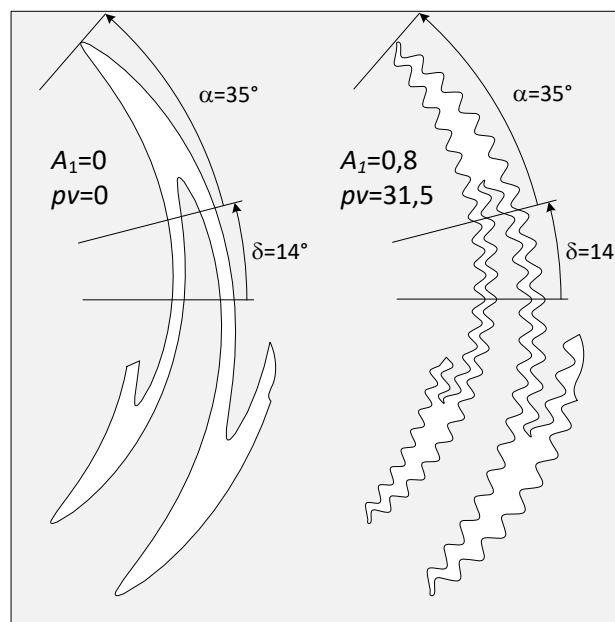


Figure 3. The cells and parameters of the antenna with and without a ripple.

To achieve the ripple of the antenna curves, it is necessary to modify Equations (3) and (4) into the following forms:

$$X(t) = t + A_1 \frac{t}{r_1 \tau^{p-1}} \cos\left(pv \frac{\pi}{\alpha} \Phi_p(t) \pm \delta\right) \cos(\Phi_p(t) \pm \delta), \tag{5}$$

$$Y(t) = t + A_1 \frac{t}{r_1 \tau^{p-1}} \cos\left(pv \frac{\pi}{\alpha} \Phi_p(t) \pm \delta\right) \sin(\Phi_p(t) \pm \delta) \tag{6}$$

where A_1 represents the relative ripple amplitude of the curves relative to the radius r in cell p . Another parameter, pv , represents the number of waves in one cell. In the antenna tuning process, several antenna modifications were created, differing in the pv parameter, which ranged from 0 to 50. The value of $pv = 0$ means that the curve in the cell is not curled but smooth (basic shape). Examples of the effect of the choice of parameter values α , δ , A_1 , and pv on the resulting shape of the contour curve are illustrated in Figure 3.

2.3. Antenna Feeding

Structures based on a micro-strip terminated with a UWB “fan” open stub [23] are generally used for feeding low-profile slot antennas. In order to minimize the reflection due to a mismatch between the feeding line and a sinuous slot, the radius and angular dimensions of the “fan” and the width of the strip must be optimized. For a lower cut-off frequency of the antenna, the radius of the “fan” increases. On the other hand, radius r_1 defines the upper frequency limit of the antenna. For frequencies that are well below 1 GHz, the “fan” radius is greater than the radius r_1 , which determines the upper frequency limit and thus also the maximum bandwidth. Therefore, a CPW was used for the excitation of the proposed antenna. The CPW is formed on the same conductive layer as the sinuous slot antenna. In the case of the CPW, the signal wire is separated from the ground by two gaps and terminated by a connection to the ground plane. The internal conductor of the CPW has a trapezoidal form. Such transmission lines behave as impedance transformers. The resulting configuration is shown in Figure 4.

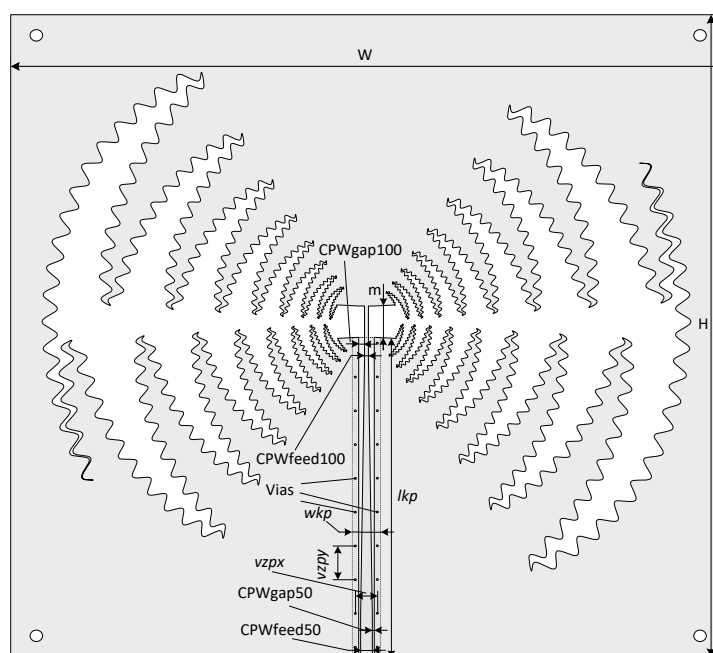


Figure 4. A model of the sinuous slot antenna: W is the printed circuit board (PCB) width, H is the PCB height.

The point of connection to the connector is the trapezoid’s widest point and its connection with the slot width, m , is the narrowest. The widest dimension of the inner conductor is denoted by CPW_{feed50} and the narrowest by $CPW_{feed100}$. The outer edges of the conductive surface have the same distance along the entire excitation length. This changes the gap between the inner and outer conductors. These gaps are similarly labeled as CPW_{gap50} and CPW_{gap100} .

The second excitation modification was the use of a coplanar waveguide with ground (CPWG) feeding. In this form of excitation, the grounding of the CPWG conductor on the other side of the substrate was connected to the base surface of the slot antenna by via holes (Vias). The width of the grounding strip on the other side of the dielectric and its length are denoted by w_{kp} and l_{kp} , respectively. The horizontal and vertical spacings are marked as vz_{px} and vz_{py} , respectively. The radius of the through-holes is denoted by r_v . Figure 4 shows the final antenna model, including both the CPWG and feeding parameters.

3. Results

To support the experiments, antennas were made in both of the forms of excitation. During the simulations, many combinations of parameters (described above) were tuned, leading to a great deal

of data. Of these, the most favorable ones were chosen, in terms of the bandwidth and minimum frequency which achieves a satisfactory parameter value, s_{11} . Figure 5 illustrates the effect of the values of the parameters α and δ as an example. From the simulation process in the frequency range of 0.1–6 GHz, it was found that the antenna design produced the best results with the selected parameters of $\delta \approx 38^\circ$ and $\alpha \approx 26^\circ$. The resulting parameters of the manufactured CPW antennas can be seen in Table 1.

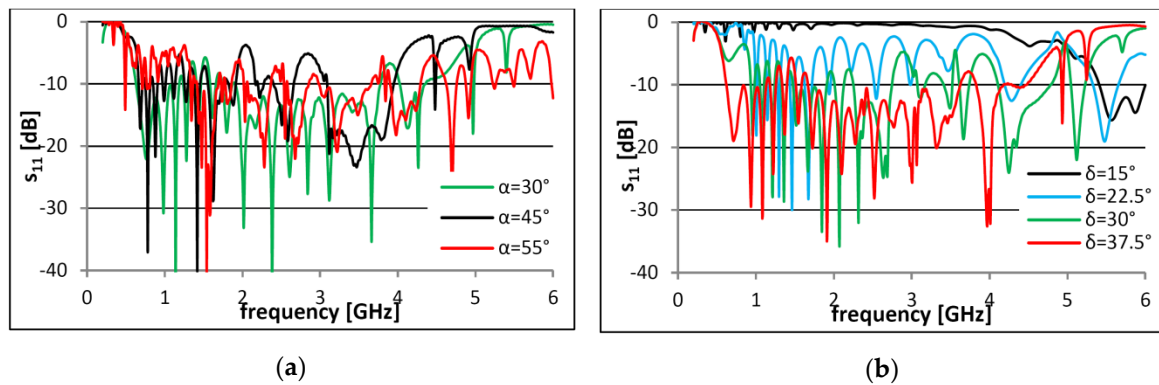


Figure 5. The simulated results (without ripples) for different values of the parameters: (a) α and (b) δ .

Table 1. The resulting parameters of the manufactured antenna with coplanar waveguide (CPW) feeding.

Parameter	Value	Parameter	Value	Parameter	Value
W	170 mm	H	160 mm	CPWfeed50	2 mm
α	26.4°	δ	38.3°	CPWgap50	0.4 mm
τ	1.151	r_1	10 mm	CPWfeed100	0.6 mm
m	4.8 mm	pv	22.1	CPWgap100	1.1 mm
A_1	1.2				

Both variants of the slotted antennas with the coplanar excitation (CPW and CPWG) were made using a subtraction method on a Rogers RO3206 substrate. Verification of the simulated characteristics of the proposed antennas was performed through standard measurement, using a vector network analyzer in an anechoic chamber (with dimensions of 5.3 m \times 3.8 m \times 3.1 m, including the RF absorber cones and shielding walls), but also using the impulse UWB radar [27]. The comparison of the measured and simulated results of the parameter s_{11} (which represents how much power is reflected from the antenna, and hence is known as the reflection coefficient or return loss) and radiation characteristics can be seen in Figures 6–10.

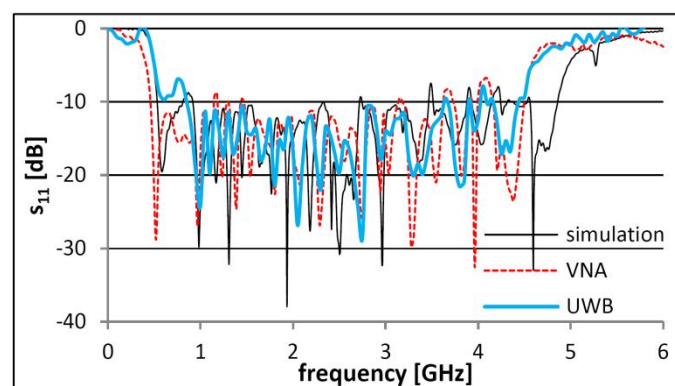


Figure 6. The simulated and measured values of parameter s_{11} for the manufactured antenna with CPW feeding.

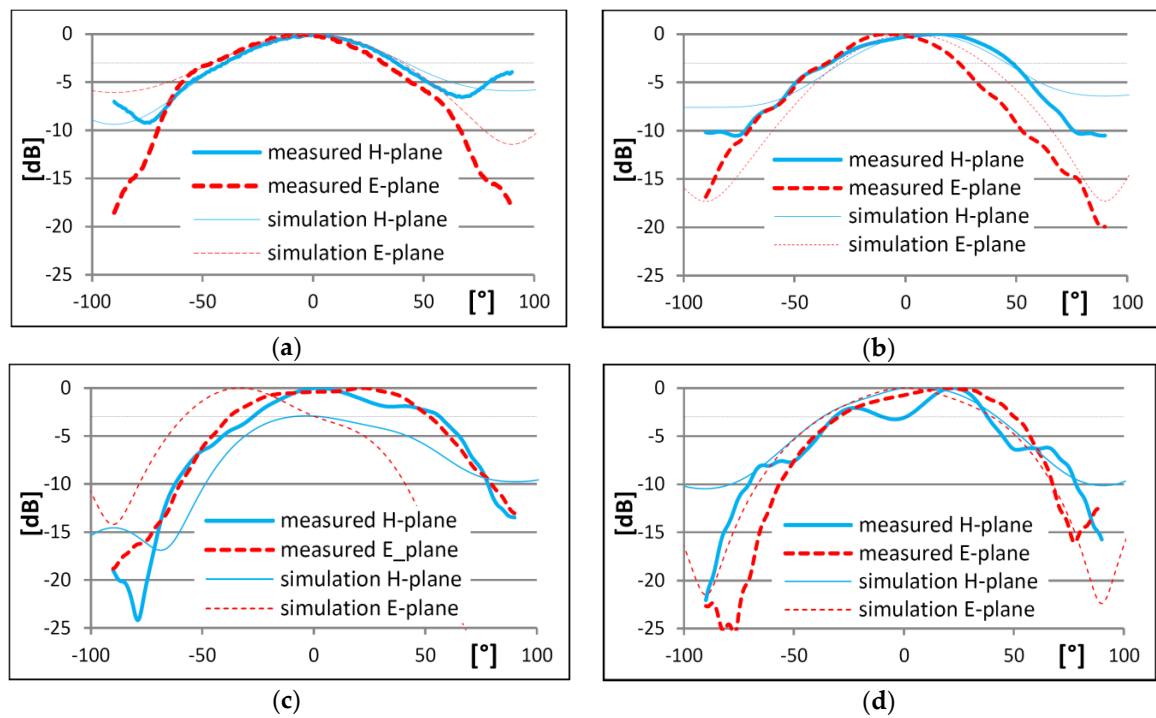


Figure 7. The antenna radiation patterns with a CPWG excitation at frequencies: (a) 1 GHz, (b) 2 GHz, (c) 3 GHz, and (d) 4 GHz.



Figure 8. Both sides of the produced sinuous slot antenna with a CPWG excitation: (a) top, (b) bottom.

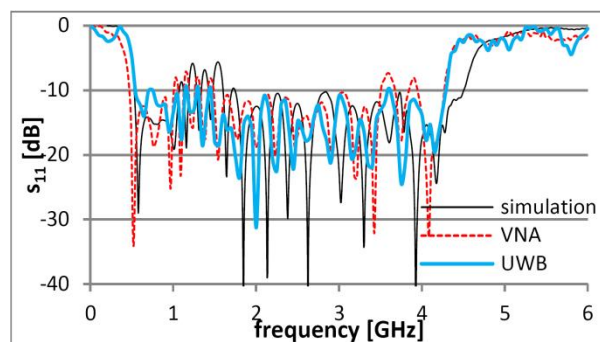


Figure 9. The simulated and measured values of parameter s_{11} for the manufactured antenna with the CPWG feeding.

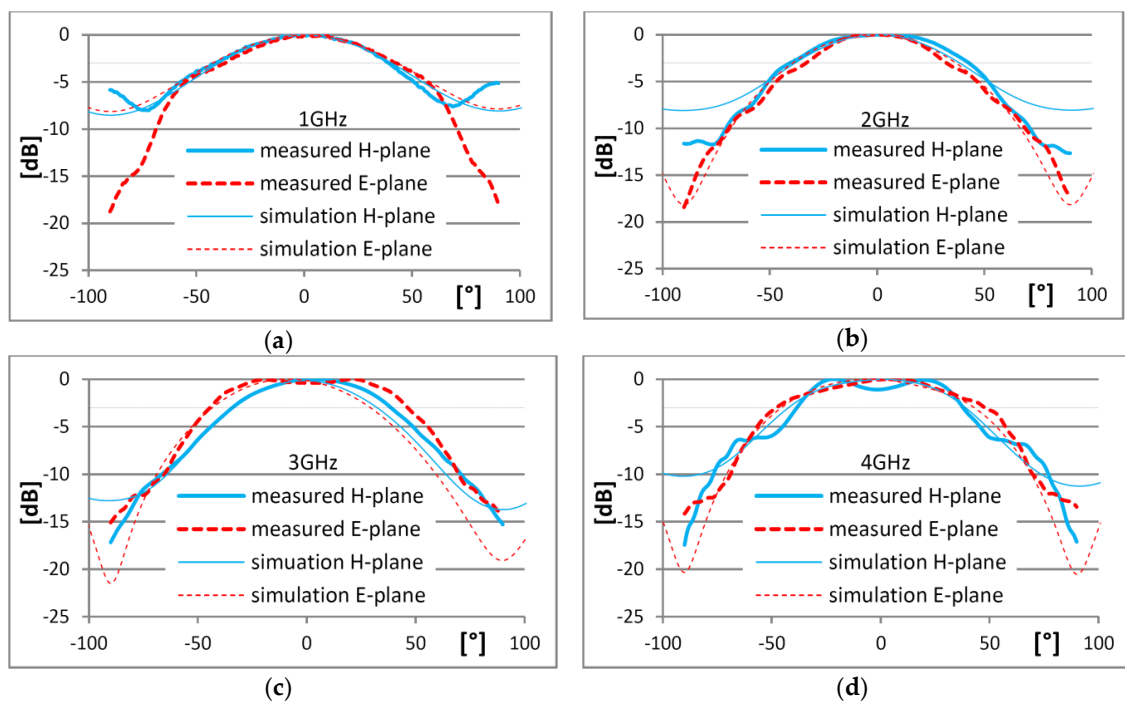


Figure 10. The antenna radiation patterns with a CPWG excitation at frequencies: (a) 1 GHz, (b) 2 GHz, (c) 3 GHz, and (d) 4 GHz.

The radiating diagrams of the antenna for the frequencies of 1–4 GHz were also simulated and measured by two methods and in two perpendicular planes, as shown in Figure 7.

Table 2 shows the dimensions and other parameters of the second version of the implemented antenna with the CPWG feeding.

Table 2. The resulting parameters of the manufactured antenna with coplanar waveguide with ground (CPWG) feeding.

Parameter	Value	Parameter	Value	Parameter	Value
W	170 mm	H	160 mm	wkp	4 mm
α	26.5°	δ	38.3°	lkp	77.65 mm
τ	1.152	r_1	10 mm	$vzpx$	3.5 mm
m	4.7 mm	pv	20	$vzpy$	3 mm
A_1	1.2	$CPWfeed50$	1.3 mm	$CPWfeed100$	0.4 mm
rv	0.2 mm	$CPWgap50$	0.55 mm	$CPWgap100$	1.0 mm

Both sides of the implemented antenna design can be seen in Figure 8.

Figure 9 compares the simulated and measured s_{11} parameters of the second antenna version (with CPWG feeding).

The measured antenna radiation patterns in the range from 1 GHz to 4 GHz, with a step of 1 GHz, are shown in Figure 10.

In our experiments, we measured the impulse response for our antennas and compared it to the available commercial antennas. The commercial antennas were QRH400 (Quad Ridged Horn Antenna) for the 0.4–6 GHz frequency band and DRH10 (Double Ridged Waveguide Horn Antenna) for the 0.74–10.5 GHz band, supplied by RFspin. Figure 11 shows the measured results for the CPWG antenna. The measurements were performed using an 8-Channel Digital Sampling Converter SD-10806 in the 0.1–6 GHz frequency range, supplied by Geozondas Ltd.

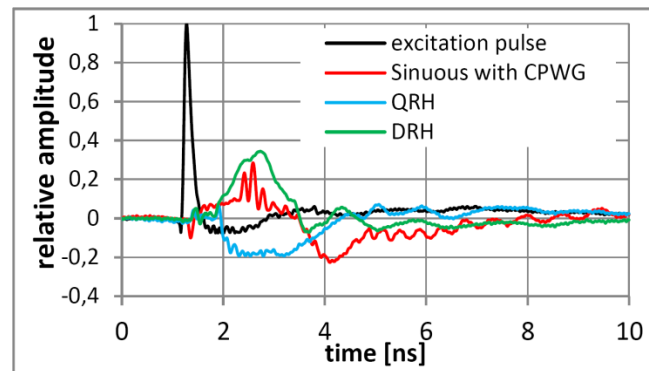


Figure 11. A comparison of the impulse response of our sinuous antenna with CPWG and the available commercial antennas in the time domain.

4. Discussion and Conclusions

This article presented the design of a UWB sinuous slot antenna intended for UWB radar applications. Several variants of the antenna were simulated, and two versions achieved sufficiently promising results to be produced as working prototypes.

By combining the coplanar waveguide and the sinuous slot antenna, a new structure was formed as an analytical curve. Choosing the parameters which defined the shape involved a wide set of tools to optimize and tune it.

The manufactured versions of the antennas differ in the way they are powered. The antennas were made in both grounded and ungrounded coplanar waveguides.

The change of the ripple amplitude was very significant in changing the s_{11} parameter (the reflection coefficient or return loss). On the one hand, in some cells, the number of ripples had a significant effect on the s_{11} result, while in other cells, this parameter had no effect. Therefore, in the embodiment shown in Figure 8, some cells are curled and others appear without a ripple.

From the simulated results for the antenna with CPW feeding (the first version), it can be seen that the frequency range of 0.53–4.86 GHz corresponds to an s_{11} value below -10 dB. Thus, it can be said that the absolute bandwidth is 4.33 GHz or the relative bandwidth is 9.1:1.

The values of parameter s_{11} obtained by measurements using a circuit analyzer showed that the working frequency band of the antenna at the -10 dB s_{11} value started at 0.459 GHz and ended at 4.5 GHz, which means the bandwidth is 4.041 GHz or, in relative terms, it is up to 9.8:1. Measurements using the UWB radar generally confirm the measured results.

The radiating patterns show that the main lobe width is about 70° and the antenna gain is within the range of 2.5–6 dBi for the listed range of frequencies.

The measured results of the second version of the antenna with CPWG excitation were also compared with the simulation results. Simulated s_{11} values showed that the antenna is suitable for the 0.53–4.5 GHz frequency band, and so the absolute bandwidth is 3.97 GHz or the relative one is 8.49:1. However, the measured s_{11} parameter determined for the antenna was in the band range of 0.459–4.29 GHz, resulting in a bandwidth of 3.831 GHz or 9.3:1. The antenna gain ranged from 2.9 to 5.7 dBi. From the antenna radiation diagrams, the width of the main lobe can be determined to be in the vicinity of 70° . However, modification of the antenna (with CPWG feeding) contributed to improving the radiation pattern's symmetry.

The measured results in both cases are better than the simulated ones. Both the resulting measured characteristics and experiments showed that these antennas are well-suited for a wide range of UWB radar applications.

From the perspective of further development, it may be said that the monolayer structure of the antenna could be suitable for development on dielectric foils or fabrics. For textile fabrics, it would be necessary to choose a technological process that would ensure a sufficient accuracy of geometric shapes

because the shape has a great effect on the antenna's impedance. In the case of dielectric films, we have a Jet Printing process in the preparation stage. Both approaches are particularly suited, for example, for wearable devices that could be used as patient monitors (heart rate, breathing) or for car drivers. In the case of drivers, such systems could be built into the seats.

Author Contributions: Conceptualization, J.G. and M.G.; methodology, J.G.; software, J.G.; validation, A.N. and C.F.; formal analysis, A.N. and C.F.; investigation, J.G.; resources, I.G.; data curation, M.R.; writing—original draft preparation, J.G.; writing—review and editing, A.N. and C.F.; visualization, P.K.; supervision, A.N.; project administration, M.G.; funding acquisition, J.G. and M.G.

Funding: Slovak authors J.G., M.R., M.G., I.G., and P.K. have been supported by the Slovak Research and Development Agency, under contract No. APVV-15-0692, and by the Science Grant Agency of the Ministry of Education Science, Research, and Sport of the Slovak Republic, under contract No. 1/0772/17.

Acknowledgments: A.N. wishes to express his sincere appreciation to the Queensland University of Technology for the opportunities provided during his exchange visit.

Conflicts of Interest: The authors declare no conflict of interest.

References

1. Fujimoto, K.; Morishita, H. *Modern Small Antennas*; Cambridge University Press: New York, NY, USA, 2014; p. 482. ISBN 978-0-521-87786-2.
2. Schantz, H.G. *The Art and Science of Ultrawideband Antennas*, 2nd ed.; Artech House: Boston, MA, USA, 2015; p. 563. ISBN 978-1-60807-955-1.
3. Staderini, E.M. UWB radars in medicine. *IEEE Aerosp. Electron. Syst. Mag.* **2002**, *17*, 13–18. [[CrossRef](#)]
4. Žiga, M.; Galajda, P.; Slovák, S.; Kmec, M. Determination of the quality of frying oil based on UWB impedance spectrometer. In Proceedings of the 16th International Radar Symposium (IRS 2015), Dresden, Germany, 24–26 June 2015; pp. 955–960.
5. Marpaung, D.H.N.; Yilong, L. A comparative study of migration algorithms for UWB GPR images in SISO-SAR and MIMO array configuration. In Proceedings of the 15th International Radar Symposium (IRS 2014), Gdansk, Poland, 16–18 June 2014; pp. 1–4.
6. Novák, D.; Zetik, R.; Kocur, D. Defective localization of target in UWB radar applications. In Proceedings of the 24th International Conference Radioelektronika 2014, Bratislava, Slovakia, 15–16 April 2014; pp. 1–4.
7. Yukhanov, Y.V.; Privalova, T.Y.; Kriuk, E.V. Characteristics of Vivaldi antennas in the radiation and scattering mode. In Proceedings of the International Conference on Electromagnetics in Advanced Applications (ICEAA 2018), Cartagena de Indias, Colombia, 10–14 September 2018; pp. 236–239.
8. Schneider, J.; Gamec, J. Overview of UWB Low-profile planar antennas. *Acta Electrotech. Inform.* **2014**, *14*, 55–59. [[CrossRef](#)]
9. Gupta, N.P.; Maheshwari, R.; Kumar, M. Advancement in ultra wideband antennas for wearable applications. *Int. J. Sci. Eng. Res.* **2013**, *4*, 341–248.
10. Elsheakh, D.M. Planar antenna for RF energy harvesting applications. In Proceedings of the 2017 IEEE International Symposium on Antennas and Propagation & USNC/URSI National Radio Science Meeting, San Diego, CA, USA, 9–14 July 2017; pp. 1171–1172.
11. Schneider, J.; Mrnka, M.; Gamec, J.; Gamcova, M.; Raida, Z. Vivaldi antenna for RF energy harvesting. *Radioengineering* **2016**, *25*, 666–671. [[CrossRef](#)]
12. Kocur, D.; Kažimír, P.; Fortes, J.; Novák, D.; Drutarovský, M.; Galajda, P.; Zetik, R. Short-range UWB radar: Surveillance robot equipment of the future. In Proceedings of the 2014 IEEE International Conference on Systems, Man, and Cybernetics (SMC 2014), San Diego, CA, USA, 5–8 October 2014; pp. 3767–3772.
13. DuHamel, R.H. Dual Polarized Sinuous Antennas. U.S. Patent 4 658 262, 14 April 1987.
14. Rahman, M.; NaghshvarianJahromi, M.; Mirjavadi, S.S.; Hamouda, A.M. Resonator based switching technique between ultra wide band (UWB) and single/dual continuously tunable-notch behaviors in UWB radar for wireless vital signs monitoring. *Sensors* **2018**, *18*, 3330. [[CrossRef](#)] [[PubMed](#)]
15. Rahman, M.; NaghshvarianJahromi, M.; Mirjavadi, S.S.; Hamouda, A.M. Bandwidth enhancement and frequency scanning array antenna using novel UWB filter integration technique for OFDM UWB radar applications in wireless vital signs monitoring. *Sensors* **2018**, *18*, 3155. [[CrossRef](#)] [[PubMed](#)]

16. Nejatijahromi, M.; NaghshvarianJahromi, M.; Rahman, M.A. New compact planar antenna for switching between UWB, narrow band and UWB with tunable-notch behaviors for UWB and WLAN applications. *Appl. Comput. Electrom.* **2018**, *33*, 400–406.
17. Rahman, M.; Ko, D.-S.; Park, J.-D. A Compact multiple notched ultra-wide band antenna with an analysis of the CSRR-TO-CSRR coupling for portable UWB applications. *Sensors* **2017**, *17*, 2174. [[CrossRef](#)] [[PubMed](#)]
18. NaghshvarianJahromi, M. Compact UWB bandnotch antenna with transmission-line-FED. *Prog. Electromagn. Res. B* **2008**, *3*, 283–293. [[CrossRef](#)]
19. Saini, K.S.; Bradley, R.F. The sinuous antenna—A dual polarized element for wideband phased array feed application. In *Electronics Division Internal Report No. 301*; National Radio Astronomy Observatory: Green Bank, WV, USA, 1996; p. 20.
20. Alotaibi, I.M.; Hong, J.; Almorqi, S.K. Cavity-backed dual linear polarization sinuous antenna with integrated microstrip balun feed. In Proceedings of the 15th Mediterranean Microwave Symposium (MMS 2015), Lecce, Italy, 30 November–2 December 2015; pp. 1–4.
21. Chen, X.; Fang, L.; Wu, X.; He, C. Design of ultra-wideband sinuous antenna applied for respiratory monitor. In Proceedings of the 2016 Asia-Pacific International Symposium on Electromagnetic Compatibility (APEMC 2016), Shenzhen, China, 17–21 May 2016; pp. 256–258.
22. Novák, D.; Schneider, J.; Kocur, D. Static person detection and localization based on their respiratory motion using various antenna types. *Acta Electrotech. Inf.* **2016**, *16*, 54–59. [[CrossRef](#)]
23. Manna, A.; Baldonero, P.; Trotta, F. Novel UWB low-profile sinuous slot antenna. In Proceedings of the 5th European Conference on Antennas and Propagation (EUCAP 2011), Rome, Italy, 11–15 April 2011; pp. 783–786.
24. Stutzman, W.L.; Thiele, G.A. *Antenna Theory and Design*, 3rd ed.; John Wiley & Sons, Inc.: Hoboken, NJ, USA, 2013; pp. 1–822. ISBN 978-0-470-57664-9.
25. Balanis, C.A. *Antenna Theory Analysis and Design*, 3rd ed.; John Wiley & Sons, Inc.: Hoboken, NJ, USA, 2005; pp. 1–1073. ISBN 0-471-66782-X.
26. Kramer, B.A.; Chen, C.-C.; Volakis, J.L. Size reduction of a UWB low-profile spiral antenna using inductive and dielectric loading. *IEEE Antenn. Wirel. Pr.* **2008**, *7*, 22–25. [[CrossRef](#)]
27. Schneider, J.; Gamec, J.; Gamcová, M.; Repko, M. Alternative antenna measuring methods with use of impulse UWB radar. In Proceedings of the 26th International Conference Radioelektronika 2016, Kosice, Slovakia, 19–20 April 2016; pp. 296–299.



© 2019 by the authors. Licensee MDPI, Basel, Switzerland. This article is an open access article distributed under the terms and conditions of the Creative Commons Attribution (CC BY) license (<http://creativecommons.org/licenses/by/4.0/>).